



HAL
open science

Measurement of the relative air permeability of compacted earth in the hygroscopic regime of saturation

Antonin Fabbri, Noha Al Haffar, Fionn Mcgregor

► To cite this version:

Antonin Fabbri, Noha Al Haffar, Fionn Mcgregor. Measurement of the relative air permeability of compacted earth in the hygroscopic regime of saturation. *Comptes Rendus. Mécanique*, 2019, 347, pp.912 - 919. 10.1016/j.crme.2019.11.017 . hal-03489107

HAL Id: hal-03489107

<https://hal.science/hal-03489107>

Submitted on 21 Jul 2022

HAL is a multi-disciplinary open access archive for the deposit and dissemination of scientific research documents, whether they are published or not. The documents may come from teaching and research institutions in France or abroad, or from public or private research centers.

L'archive ouverte pluridisciplinaire **HAL**, est destinée au dépôt et à la diffusion de documents scientifiques de niveau recherche, publiés ou non, émanant des établissements d'enseignement et de recherche français ou étrangers, des laboratoires publics ou privés.



Distributed under a Creative Commons Attribution - NonCommercial 4.0 International License

Measurement of the air relative permeability of compacted earth in the hygroscopic regime of saturation

Antonin Fabbri^{a,*}, Noha Al Haffar^a, Fionn McGragor^a

^a*LTDS, UMR 5513 CNRS, ENTPE, 69100 Vaulx-en-Velin, France*

Abstract

The hygroscopic behavior of earthen materials has been extensively studied in the past decades. However, while air flow within their porous network may significantly affect the kinetic of vapor transfer and thus their hygroscopic performances, few studies have focused on its assessment. For that purpose, a key parameter would be the gas permeability of the material, and its evolution with the air relative humidity. Indeed, due to the sorption properties of earthen material, an evolution of the water content, and thus of the relative permeability, are foreseeable if the humidity of in-pore air changes. To fill this gap, this paper presents the measurement of relative permeabilities of a compacted earth sample with a new experimental set-up. The air flow through the sample is induced with an air generator at controlled flow rate, temperature and humidity. The sample geometry was chosen in order to reduce, as much as possible, its heterogeneity in water content and the tests were realized for several flow rates. The results, which show the evolution of gas permeability with the relative humidity of the injected air and with the water content of the material, either in adsorption or in desorption, were eventually successfully compared to predictions of the well known Corey's law.

Keywords: Earthen materials; Relative permeability; Steady-state; Darcy's law; Vapor advection

*Corresponding author

1. Introduction

In the general context of global warming, earthen constructions are regaining interest mainly due to their attractiveness in terms of their low embodied energy [28, 1] and for their high potential to contribute to a passive regulation of the interior climate of dwellings and other buildings [20, 32, 23, 7]. Each construction can potentially be built with a different material and cannot be totally included in an industrial process. Therefore, several construction techniques have been invented adapting them to the nature of the soil used. Among these techniques the three most common ones are adobe blocks, cob and rammed earth [21].

But, whatever the construction technique, strong similarities exist in the soils used. For instance, all earthen materials used are described as a porous media with a relatively high permeability and with a solid matrix composed of non-negligible amount of clays, therefore, allowing good vapor sorption properties [26]. The affinity of earthen materials to water also induces substantial complexity in their mechanical behavior. Indeed, in addition to the drop in strength commonly observed at high water content values [5], recent studies have underlined that significant changes in the mechanical behavior (strength variations, shrinkage, swelling) may be observed under normal operating conditions due to the modification of air relative humidity [9, 33, 4]. In consequence, a first step to correctly assess the behavior of earthen walls is the precise quantification of the humidity field within the in-pore air and within the material. [15].

For that purpose, the main equations which describe the hygroscopic couplings are nowadays quite well known by the scientific community (cf. [24, 31] for example). But, one of the main challenges remains the proper estimation of the material parameters which drive these mass transports equations, such as the vapor transfer coefficient [25], the isothermal sorption-desorption curve [14, 6], as well as the liquid and gas relative permeabilities [16].

In particular, the increasing development of research activities on mass transfer through earthen materials has highlighted the strong lack in literature of measurements of gas relative permeability in the hygroscopic range of saturation.

This can be explained by the fact that advection of vapor due to gas transport is almost always neglected. But this quite common simplification has not got any consensus since some authors have already underlined that air flows may have a significant impact on the hygroscopic behavior of porous material like
35 concrete [2], textiles [18], or even earthen and bio-based materials [3].

In this context, this paper presents the development of an experimental set up to measure the relative permeabilities of a compacted earth sample. The air flow through the sample was induced with a humid air generator at controlled flow rate, temperature and humidity. The testing protocol, including the defini-
40 tion of the sample geometry, is presented in the first part. Then, the results of gas permeability as function of relative humidity of the injected air and water content, either in adsorption or in desorption, are presented and compared to predictions of the well known Corey's law [10].

2. Material characterization and preparation

45 2.1. Raw earth material and sample realization

The earthen material presented in this study is sampled from rammed earth walls of an existing construction located in the South-East of France during operations of opening new doors and windows. This choice ensures that the studied material is suitable for building sustainable earth constructions. Parti-
50 cle size distribution, Atterberg limits and methylene blue value were measured. It shows a mass content of clay (particles with a diameter lower than $2 \mu\text{m}$) equal to 16%, a plasticity index of 14% and a blue value of 2.7.

Cylindrical samples of 3.5 cm in diameter and 7 cm high were manufactured
55 at the optimum moisture content resulting in maximum dry density (11% and 1.97 g/cm^3). Those parameters were previously determined using a manual CEB press. More details on the sample realization protocol are given in [9]. Just after their production, the samples were dried at 23°C in a desiccator with silica gel until a constant mass was reached. The relative humidity within the

60 desiccator was checked with a portable sensor (Rotronic HygroLog HL-NT), and it was found to be consistently lower than 5% RH.

2.2. Porous and hygroscopic properties

After the drying period, the cylinders were weighed and measured in order to estimate their dry density. Their specific density and their porosity were measured with a nitrogen pycnometer. The obtained values are reported in the 65 Table 1.

Adsorption-desorption curves were measured using the Dynamic gravimetric Vapor Sorption method, commonly called the DVS method. It consists in measuring uptake and loss of moisture by flowing a carrier gas at a specified relative 70 humidity (or partial pressure) over a small sample (from several milligrams to several grams depending on the device used) suspended from the weighing mechanism of an ultrasensitive recording microbalance. Variations in the gas's relative humidity are automatically calculated by the device when the target condition in mass stability is reached. Results are reported in the Figure 1.

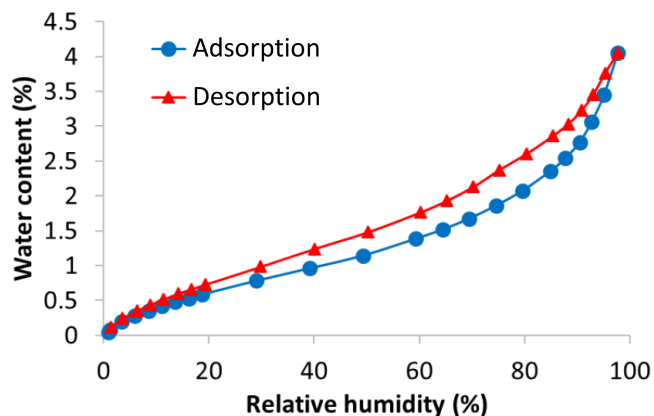


Figure 1: Adsorption and desorption curves at 23°C of the tested material obtained with the DVS method.

75 Water vapor permeability was measured using the wet cup method following the procedure described in [25]. The vapor pressure gradient is created for the

wet cup by setting the RH at 60% in the chamber and 85% in the cup. It leads to the values reported in the Table 1.

Symbol	Description	Value [unity]
ϕ	Porosity	0.26
ρ_d	Dry density	1.97 [g/cm ³]
ρ_s	Specific density	2.7 [g/cm ³]
δ_p	diffusion coefficient of vapor	4.2×10^{-11} [kg/m/Pa/s]

Table 1: Hygroscopic parameters of the samples.

80 Since this study focuses on the hygroscopic regime of saturation (saturation degree lower than 20%) the impact of liquid water transport was neglected and the liquid permeability was not measured.

3. Experimental method to measure the gas permeability

3.1. Intrinsic and relative permeability

85 The gas permeability, denoted by κ_G , characterizes the ability of a fluid mass to move through the porosity of a material. For an isotropic medium, and neglecting the influence of gravity, mass flow of gas writes in the form:

$$\underline{\omega}_G = -\rho_G \frac{\kappa_G}{\eta_G} \underline{\nabla} P_G \quad (1)$$

where $\underline{\omega}_G$ is the mass flow vector, η_G is the viscosity of the gas, P_G its pressure and ρ_G its density, which is assumed to satisfy the perfect gas relation:

$$\rho_G = \frac{M_G}{RT} P_G \quad (2)$$

90 The value of the gas permeability depends on the geometry of the porous network, which may change when the material deforms, and on the volumetric proportion of the pore space occupied by adsorbed and/or condensed water

molecules [27]. The present study is limited to unloaded materials, which remain in the hygroscopic range of saturation. Thus the impact of the material
95 deformation can reasonably be neglected and, for an isotropic medium, the gas permeability can be written in the form:

$$\kappa_G = \kappa_G^0 \kappa_G^r(w) \quad (3)$$

where κ_G^0 is the intrinsic permeability, that is the gas permeability for a totally dried sample, and $\kappa_G^r(w)$ is the relative permeability, which is function of the water content, denoted by w . For the record, the water content is defined as
100 the mass of water divided by the dry mass of the solid.

3.2. Set up of experimental device

Several methods exist to estimate the intrinsic permeability. Mainly transient methods [11] or steady-state methods [29]. Indirect estimation methods, based on the upscaling of transfers within the interconnected pores at several
105 levels have also been developed [8].

In this paper, a steady-state approach is chosen. When low saturation ratios are considered, the main difficulty of this method is to be able to generate flows of gas and/or liquid while keeping a constant and homogeneous saturation state through the sample. To overcome this problem, one method, already used to
110 assess the liquid relative permeability of cement based materials [34] and gas relative permeability of textiles [17], consists in fixing the water content of the material through the relative humidity of the incoming air. Indeed, as it is depicted by the sorption curves (cf. Figure 1), any increase of air relative humidity will increase its water content.

115

For that purpose, an experimental device quite similar to the one developed by Gibson et al. [17] for textiles applications was set up. It is made of a static triaxial cell (GDS/CEL/STA/100) with drainage systems on its cap and base pedestal. They are linked to a wet air generator (WETSYS S60/59105) at
120 constant flow rate, varying between 5mL/min to 200mL/min depending on the

relative humidity, which varies between 0% and 95% and a temperature between ambient and 50°C. A special climatic chamber was built to contain the cell and regulate its temperature (accuracy of 0.1°C). The wet air can be injected in the sample through its bottom side or its top side, while the other side is kept
 125 at atmospheric pressure. The inlet/outlet pressures, temperatures and relative humidity are monitored during the whole test. A diagram of the experimental device is reported in the Figure 2.

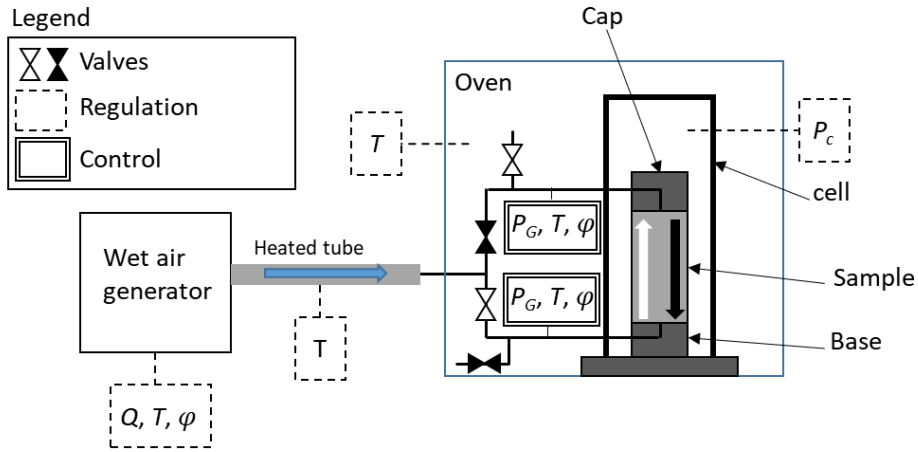


Figure 2: Schematic diagram of the experimental device. The black arrow through the sample represent the direction of the gas flow when the black valves are open and the white valves are closed, and reciprocally for the white arrow. P_c is the confinement pressure in the cell, T the temperature, Q the volumetric flow rate, φ the relative humidity and P_G the gas pressure.

Using this device, the gas at controlled relative humidity was injected at constant flow rate within the material. Difference between inlet and outlet
 130 pressures, respectively denoted by $P_{G,i}$ and $P_{G,o}$, was recorded. When this latter became constant, the steady state was assumed to be reached. To ensure an unidirectional flow and to avoid leakage at the interfaces with the base and the cap, the sample was jacketed in an impermeable latex membrane, and a confinement pressure of 1bar is applied, which remains at least twice the inlet

135 overpressure. Given the bulk modulus of the materials, which is higher than
 300 MPa even for a relative humidity of 97% [33], the volumetric strain induced
 by the confinement pressure is in the order of 10^{-4} , therefore the impact on
 transport properties is assumed to be negligible.

140 *3.3. Principle of measurement, sample geometry and the maximum flow rate*

Under steady-state condition, if the water content is homogeneous through
 the sample, the mass conservation of the gas phase (that is $\underline{\nabla} \cdot \underline{\omega}_G = 0$), combined
 with (1-2) leads to:

$$\kappa_G = \kappa_0 \kappa_G^r(w) = Q \eta_G \frac{2HP_{G,i}}{A(P_{G,i}^2 - P_{G,o}^2)} \quad (4)$$

where H is the sample thickness, A its cross surface and Q is the incoming vol-
 145 umetric gas flow rate ($Q = \rho_{G,i} \underline{\omega}_G \cdot \underline{n}$, with $\rho_{G,i}$ is the gas density of incoming
 gas and \underline{n} the outgoing normal vector).

On the other side, if the water content is not homogeneous though the sam-
 ple, the mass conservation of the air does not directly provide the permeability,
 150 but its average value. In consequence, a good control of the heterogeneity in
 water content, and thus of the air relative humidity, through the sample is nec-
 essary for an accurate measurement of the gas permeability. For that purpose,
 the flow of vapor mass within the sample, which is denoted by $\underline{\omega}_V$, must be
 assessed precisely. Considering both vapor advection and diffusion processes,
 155 $\underline{\omega}_V$ satisfies:

$$\underline{\omega}_V = \frac{\rho_V}{\rho_G} \underline{\omega}_G - P_G \delta_p \underline{\nabla} \left(\frac{\varphi p_V^s}{P_G} \right) \quad (5)$$

where φ is the relative humidity of the in-pore air, p_V^s the vapor pressure at
 saturation and ρ_V its apparent density, which is assumed to satisfy the perfect
 gas relation:

$$\rho_V = \frac{M_w}{RT} \varphi p_V^s \quad (6)$$

In (5), the term $(\rho_V/\rho_G)\underline{\omega}_G$ represents the mass of vapor advected by the
 160 gas phase, while $-P_G\delta_p\underline{\nabla}(p_V/P_G)$ is the diffusion of vapor within the gas phase.
 If the incoming flow of air is in the order of 10mL/min, the order of magnitude
 of the mass of vapor advected by the gas phase within the sample of cross section
 $A = 10\text{cm}^2$ is 10^{-5}kg/s/m^2 . On the other side, considering the material
 parameters of the table 1, the diffusive flow for a variation of relative humidity
 165 of 0.1 within a 1cm thick sample is in the order of 10^{-6}kg/s/m^2 . At first, order,
 this latter can thus be neglected.

Under this assumption, the combined use of the relations (1-6), the mass con-
 servation equations ($\underline{\nabla} \cdot \underline{\omega}_G = 0$ and $\underline{\nabla} \cdot \underline{\omega}_V = 0$), and the relation (4) allows
 to express the relative difference between outlet and inlet relative humidity at
 170 constant temperature, denoted by r_φ , in the form:

$$r_\varphi = \frac{\varphi_o - \varphi_i}{\varphi_i} = \frac{1}{\chi} \left(\sqrt{1 + \chi^2} + 1 \right) - 1 \quad (7)$$

where φ_o and φ_i are respectively the outlet and the inlet relative humidity
 while χ is a dimensionless number, which is a function of the permeability of
 the material, its geometry (thickness and cross section), of the flow rate and of
 the outlet pore pressure. It is equal to:

$$\chi = \frac{\kappa_0 < \kappa_G^r > AP_{G,o}}{\eta_G QH} \quad (8)$$

The evolution of r_φ with χ is reported in the Figure 3. To insure a good ho-
 mogeneity in water content through the sample, r_φ must be as low as possible,
 and thus χ must be as high as possible.

175 Since the outlet pressure and the sample surface are fixed, the only parame-
 ters on which it is possible to act to increase χ are the gas flow and the sample
 thickness, which should be both as small as possible. The lower flow rate that
 can be reached while keeping a good regulation with our system is 10mL/min.
 On the other side, in order to avoid too important inlet overpressure, Q will be
 180 limited at 25mL/min.

Under these conditions, and assuming permeability values higher than 1×10^{-14}

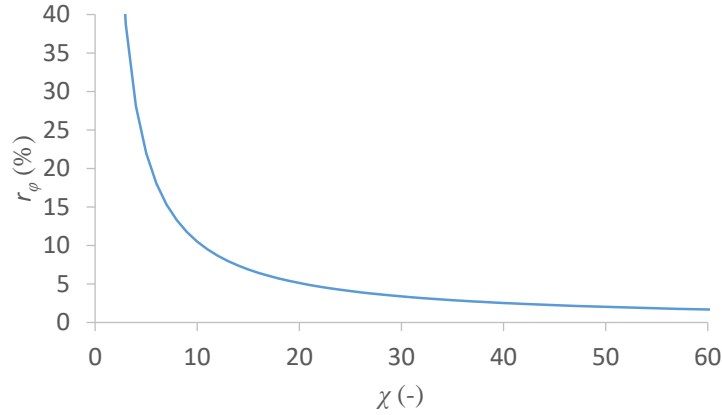


Figure 3: Evolution of r_φ with χ .

m^2 , a sample thickness of 1cm would lead to values of χ higher than 12.7 and r_φ lower than 8%. This relative variation, which is range of uncertainties of the relative humidity sensors, is considered as acceptable.

185 *3.4. Test protocol*

The first stage consist in applying through the sample a flow of dry air at 25mL/min. When the permanent state is reached (stable relative humidity and pressure at inlet and outlet), the flow is progressively reduced to 10mL/min by steps of 5mL/min. For each step, the inlet and outlet pressures were recorded
 190 and the permeability coefficient was estimated using the equation (4) as long as the permanent state was reached. Even if permeability measurements were made at different flows, the outlet overpressure remained equal to 0, while the inlet overpressure was limited to 0.5 bar. Due to these technical constrains, the mean pressure variations remained quite limited and it was not possible
 195 to study the Klinkenberg's effect [22]. In consequence, only the apparent gas permeability was measured in this study.

4. Results of gas permeability measurements

Gas permeabilities measured for all testing configurations are summarized in the Table 2. At first, the tests performed at the several flow rates underline its
200 limited impact in the range of values considered in this study (that are between 10mL/min and 25mL/min). This result gives some confidence on the accuracy of measurements, particularly with regard to those of inlet and outlet pressures. Whatever the relative humidity of the injected air, permeabilities in the range of 10mD (10^{-14}m^2) were observed. It emphasizes the permeable nature of the
205 tested material. Indeed, it is in the range of gas permeability of permeable rocks like Voges sandstones [30], while being at least three orders of magnitude higher than that of cement based materials [13].

This result is interesting by itself. Indeed, given this high value of gas permeability, the mass transfer of vapor through the material by air advection process
210 might not be negligible if gas pressure variations, caused by wind effect for example, are considered. Anyway, it underlines that this point deserves to be analyzed.

Nonetheless, even if they remained in the same order of magnitude, a noticeable reduction of the gas permeability was observed when the relative humidity
215 of the injected air increases. For the record, injection of dry air led to permeabilities 35% higher than injection of wet air at 90%HR. This variation may not be negligible if in-pore vapor advection need to be considered to have a correct estimation of the humidity field within the material, especially since it is in the range of relative humidity that may be observed during the lifetime of
220 an earthen wall.

To analyze further these results, the average relative humidity, defined as the arithmetic mean between the inlet and outlet relative humidity, was rather considered. It is supposed to be representative of the average humidity within
225 the sample. Due to the quite limited gradient of relative humidity within the sample, this approach, though simplified, is considered sufficient.

The variation of gas permeability with the average relative humidity is reported in the Figure 4A. Interestingly, a difference is observed between the permeabilities which were measured during adsorption and desorption stages. Because
 230 gas permeability should rather be driven by the water content than by air relative humidity (cf. eq. (3)), this may be a consequence of the hysteresis between adsorption and desorption curves as it is depicted in the Figure 1. This assumption seems verified by the results presented in the Figure 4B, in which almost
 235 no more difference was observed between adsorption and desorption stages if the gas permeability is expressed as function of the water content instead of the relative humidity. For this graph, the water content was not directly measured, but it was calculated from the average relative humidity and using either the adsorption or the desorption curves depending on the stage which is considered.

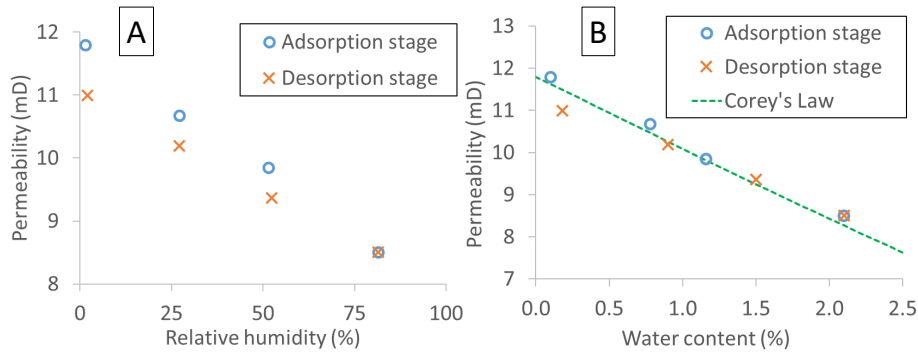


Figure 4: Evolution of the gas permeability with relative humidity (A) and water content (B). The permeability is expressed in mD ($1\text{mD} \approx 1.0 \cdot 10^{-15} \text{ m}^2$)

240 **5. Discussion on the evolution of air relative permeability with liquid saturation**

The variation of gas permeability with water saturation can be attributed to several phenomena A first one, which was already observed in textile materials by [19], can be the modification of the microstructure due to swelling processes.

245 However, this explanation might not be consistent with the quite limited volumetric swelling, lower than 0.005%/rh, which was measured in [12] for similar compacted earth samples (same earth, similar dry density, same compaction procedure).

A second explanation can rise up from the analysis of the porous network structure of the material. As it was discussed in [16], it should be composed by large pores connected to each others by narrow throats. Adsorption of water molecules at the pore walls when air relative humidity increases may thus fill some of these narrow throats. As a consequence, the number of percolation pathways through the material for the gas phase would be reduced, which translates, at the macroscopic scale, by a reduction of the gas permeability. To go further on that point, it could be interesting to analyses more in detail the shape of the relation between the gas permeability and the liquid ratio. For that purpose, several theoretical and empirical laws have been already developed [11]. Among them, one of the most used is the Corey's law [10], which writes in the form:

$$\kappa_G = \kappa_G^0 (1 - S_r)^2 (1 - S_r^2) \quad (9)$$

where S_r is the reduced saturation ratio, which can take into account the impact of both liquid and gas residual saturation. If these two terms are considered to be null and, if the deformation of the material is neglected, S_r can be linked to the water content, denoted by w , through the relation:

$$S_r = w \frac{\rho_d \rho_s}{\rho_s - \rho_d} \quad (10)$$

250 The comparison between the predictions obtained with the relations (9-10) and the experimental results is reported in the Figure 4B. A good consistency is observed even though no calibration parameters were used since both residual liquid and gas saturation were assumed to be null.

255 Even if it is not a formal proof, the fact that Corey's law was initially established from experimental data of non-swelling porous materials and for oil

and gas in-pore phases (instead water and air) tends to give some confidence on the assumption that the variation of permeability is rather induced by filling of some narrow pores with liquid water than by swelling phenomena.

260

Finally, to interpret properly this result it is important to underline that, for a given hydric state, water content value depends on the method which is used to reach the reference dry state of the sample (that is for which $w = 0$). For example, it was shown in [14] that earthen samples will have a lower mass after
265 being dried in an oven at 105°C than after being dried by a flow of dry air at 23°C. In this study, a flow of dry air at 23°C was used to determine the dry mass of the samples. In consequence, to obtain same results while considering a dry mass from oven-drying at 105°C, it would be necessary to take into account a non-null residual saturation in the expression of S_r . In view of the definition of a
270 standardized method to estimate a consistent dry mass of earthen materials, this results, although it needs to be further investigated, may be quite interesting.

6. Conclusion

In this paper, a novel apparatus to measure the evolution of the gas permeability of earthen material in the hygroscopic range of saturation was presented.
275 From the analysis of the water vapor transport within the porous network of the material, limits on sample thickness and flow rate of the injected wet air were determined. The obtained results were analyzed in terms of water content and relative humidity. The Corey's law was found to fit accurately the experimental results, without the needs of any calibration parameters. In consequence, at
280 least for the same kind of sample than the one studied here (compacted fine earth with no gravels, quite high dry density), a single measurement of the intrinsic gas permeability can be sufficient to estimate the variation of the gas permeability with water content in the hygroscopic range of saturation.

References

- 285 [1] Arrigoni A, Beckett C, Ciancio D and Dotelli G (2017) Life cycle analysis of environmental impact vs. durability of stabilised rammed earth. *Construction and Building Materials* **142**: 128–136.
- [2] Baroghel-Bouny V, Mainguy M, Lassabatere T and Coussy O (1999) Characterization and identification of equilibrium and transfer moisture properties
290 for ordinary and high-performance cementitious materials. *Cement and Concrete Research* **29**: 1225–1238.
- [3] Berger J, Gasparin S, Dutykh D and Mendes N (2018) On the solution of coupled heat and moisture transport in porous material. *Transport in Porous Media* **121**: 665–702.
- 295 [4] Bruno A, Perlot C, Mendes J and Gallipoli D (2018) A microstructural insight into the hygro-mechanical behaviour of a stabilised hypercompacted earth. *Materials and Structures* **51**: 32.
- [5] Bui QB, Morel JC, Hans S and Walker P (2014) Effect of moisture content on the mechanical characteristics of rammed earth. *Construction and*
300 *Building Materials* **54**: 163–169.
- [6] Bui R, Labat M and Aubert J (2017) Comparison of the saturated salt solution and the dynamic vapor sorption techniques based on the measured sorption isotherm of straw. *Construction and Building Materials* **141**: 140–151.
- 305 [7] Busser T, Pailha M, Piot A and Woloszyn M (2019) Simultaneous hygrothermal performance assessment of an air volume and surrounding highly hygroscopic walls. *Building and Environment* **148**: 677–688.
- [8] Carmeliet J, Descamps F and Houvenaghel G (1999) A multiscale network model for simulating moisture transfer properties of porous media. *Transport in*
310 *porous media* **35**: 67–88.

- [9] Champiré F, Fabbri A, Morel J, Wong H and McGregor F (2016) Impact of hygrometry on mechanical behavior of compacted earth for building constructions. *Construction and Building Materials* **110**: 70–78.
- [10] Corey A (1954) The interrelation between gas and oil relative permeability. *Producers Monthly* **19**: 38–41.
- [11] Dana E and Skoczylas F (1999) Gas and stones permeability and pore structure of sandstones. *International Journal of Rock Mechanics and Mining Science* **36**: 613–625.
- [12] Fabbri A, Champiré F, Soudani L, McGregor F and Wong H (2017) Poromechanics of compacted earth for building applications. *Poromechanics 2017 - Proceedings of the 6th Biot Conference on Poromechanics* .
- [13] Fabbri A, Corvisier J, Schubnel A, Brunet F, Goffé B, Rimmelé G and Barlet-Gouédard V (2009) Effect of carbonation on the hydro-mechanical properties of portland cements. *Cement and Concrete Research* **39**: 1156–1163.
- [14] Fabbri A, McGregor F, Costa I and Faria P (2017) Effect of temperature on the sorption curves of earthen materials. *Materials and Structures* **50**: 253.
- [15] Fabbri A, Morel J and Gallipoli D (2018) Assessing the performance of earth building materials: a review of recent developments. *RILEM Technical Letters* **3**: 46–58.
- [16] Fabbri A, Soudani L, McGregor F and Morel J (2019) Analysis of the water absorption test to assess the intrinsic permeability of earthen materials. *Construction and Building Materials* **199**: 154–162.
- [17] Gibson P and Charmchi M (1997) Modeling convection/diffusion processes in porous textiles with inclusion of humidity-dependent air permeability. *International Communications in Heat and Mass Transfer* **24**: 709–724.

- [18] Gibson P, Elsaid A, Rivin CKD and Charmchi M (1997) A test method to determine the relative humidity dependence of the air permeability of textile materials. *Journal of Testing and Evaluation* .
- [19] Gibson P, Rivin D, Kendrick C and Schreuder-Gibson H (1999) Humidity-dependent air permeability of textile materials. *Textile Research Journal* **69**: 311–317.
- [20] Hall M and Allinson D (2009) Analysis of the hygrothermal functional properties of stabilised rammed earth materials. *Building and Environment* **44**: 1935–1942.
- [21] Hall M and Krayenhoff RL (2012) *Modern earth buildings*. Woodhead.
- [22] Klinkenberg J (1941) The permeability of porous media to liquids and gases. *Drilling and Production Practice* .
- [23] Labat M, Magniont C, Oudhof N and Aubert J (2016) From the experimental characterisation of the hygrothermal properties of straw-clay mixtures to the numerical assessment of its buffering potential. *Building and environment* **97**: 69–81.
- [24] Labat M and Woloszyn M (2016) Moisture balance assessment at room scale for four cases based on numerical simulations of heat/air/moisture transfers for a realistic occupancy scenario. *Journal of Building Performance Simulation* **9**: 487–509.
- [25] McGregor F, Fabbri A, Ferreira J, Simoes T, Faria P and Morel JC (2017) Procedure to determine the impact of the surface film resistance on the hygric properties of composite clay/fibre plasters. *Materials and Structures* **50**.
- [26] McGregor F, Heath A and Shea A (2014) The moisture buffering capacity of unfired clay masonry. *Building and Environment* **82**: 599–207.
- [27] Monfared M, Sulem J, Delage P and Mohajerani M (2014) Temperature and

damage impact on the permeability of opalinus clay. *Rock Mechanics and Rock Engineering* **47**: 101–110.

- [28] Morel J, Mesbah A, Oggero M and Walker P (2011) Building houses with local materials: means to drastically reduce the environmental impact of construction. *Buildings and Environment* **36**: 1119–1126.
- [29] Osselin F, Fabbri A, Fen-Chong T, Pereira J, Lassin A and Dangla P (2015) Experimental investigation of the influence of supercritical state on the relative permeability of vosges sandstone. *Comptes Rendus Mecanique* **343**: 495–502.
- [30] Osselin F, Fen-Chong T, Fabbri A, Lassin A, Pereira J and Dangla P (2013) Dependence on injection temperature and on aquifer’s petrophysical properties of the local stress applying on the pore wall of a crystallized pore in the context of CO₂ storage in deep saline aquifers. *The European Physical Journal Applied Physics* **64**: 21101.
- [31] Soudani L, Fabbri A, Morel J, Woloszyn M, Chabriac P, Wong H and Grillet A (2016) A coupled hygrothermal model for earthen materials. *Energy and Buildings* **116**: 498–511.
- [32] Woloszyn M, Kalamees T, Abadie M, Steeman M and Kalagasidis AS (2009) The effect of combining a relative-humidity-sensitive ventilation system with the moisture buffering capacity of materials on indoor climate and energy efficiency of buildings. *Building and Environment* **44**: 515–524.
- [33] Xu L, Wong K, Fabbri A, Champiré F and Branque D (2018) Loading-unloading shear behavior of rammed earth upon varying clay content and relative humidity conditions. *Soils and Foundations* **58**: 1001–1015.
- [34] Zamani S, Kowalczyk R and McDonald P (2014) The relative humidity dependence of the permeability of cement paste measured using nmr profiling. *Cement and Concrete Research* **57**: 88–94.

φ_i [%]	Q [mL/min]	φ_{moy} [%]	$\Delta\varphi$ [%]	κ_G [mD]
Adsorption stage				
0.5	24.88	1.1	1.3	11.74
0.5	19.97	1.2	1.4	11.76
0.8	14.64	1.4	1.2	11.6
1.8	9.80	2.3	0.4	12.1
29.1	24.67	26.7	4.8	10.68
29.2	19.75	26.8	4.8	10.61
30.0	14.76	27.2	5.6	10.64
29.5	9.78	27.2	4.7	10.77
57.0	24.67	52.0	10.0	9.94
56.8	19.46	52.0	9.6	9.83
56.7	14.67	51.9	9.6	9.80
56.4	9.66	51.6	9.6	9.90
90.9	24.62	81.5	18.8	8.61
88.9	19.46	80.6	16.7	8.49
91.4	14.67	81.7	19.3	8.42
91.3	9.66	81.5	19.7	8.49
Desorption stage				
57.3	24.67	52.8	9.0	9.41
57.8	19.75	53.0	9.6	9.37
58.5	14.71	53.3	10.5	9.29
57.4	9.69	52.4	9.9	9.38
29.6	24.96	27.3	4.7	10.24
29.2	19.61	27.2	4.1	10.03
29.2	14.67	27.2	4.1	10.01
29.2	9.71	27.2	4.0	10.50
0.3	24.85	1.1	1.5	11.02
0.7	19.84	2.0	2.5	10.91
1.2	14.92	2.3	2.1	10.93
1.9	9.91	2.7	1.7	11.12

Table 2: Summary of the results obtained for the several relative humidity and air flow. φ_{in} is the relative humidity of the injected air, φ_{moy} is the average between the inlet and outlet relative humidity while $\Delta\varphi$ denotes the difference between the inlet and outlet relative humidity.